
It’s FLAN time! Summing feature-wise latent representations for interpretability

An-phi Nguyen
IBM Research Europe, ETH Zürich

Stefania Vasilaki
ETH Zürich

Maria Rodríguez Martínez
IBM Research Europe

Abstract

Interpretability has become a necessary feature for machine learning models deployed in critical scenarios, e.g. legal system, healthcare. In these situations, algorithmic decisions may have (potentially negative) long-lasting effects on the end-user affected by the decision. In many cases, the representational power of deep learning models is not needed, therefore *simple and interpretable* models (e.g. linear models) should be preferred. However, in high-dimensional and/or complex domains (e.g. computer vision), the universal approximation capabilities of neural networks are required. Inspired by linear models and the Kolmogorov-Arnold representation theorem, we propose a novel class of *structurally-constrained* neural networks, which we call FLANs (Feature-wise Latent Additive Networks). Crucially, FLANs process each input feature *separately*, computing for each of them a representation in a common latent space. These feature-wise latent representations are then simply *summed*, and the aggregated representation is used for prediction. These constraints (which are at the core of the interpretability of linear models) allow a user to estimate the effect of each individual feature *independently* from the others, *enhancing interpretability*. In a set of experiments across different domains, we show how without compromising excessively the test performance, the structural constraints proposed in FLANs indeed facilitates the interpretability of deep learning models. We quantitatively compare FLANs interpretability to post-hoc methods using recently introduced metrics, discussing

the advantages of natively interpretable models over a post-hoc analysis.

1 INTRODUCTION

The recent surge in interest towards *interpretable machine learning* research can arguably be attributed to the success of deep learning models. Despite their universal approximation capabilities (Cybenko, 1989; Hornik et al., 1989) and generalization properties (Kawaguchi et al., 2017; Arora et al., 2018), these models often behave as a black-box from a user perspective: their “decision process” is often unclear, especially to layman users. While not always necessary, interpretability can be *critical* in applications with far-reaching impact, e.g. in legal cases and healthcare. In these high-stake scenarios, (Rudin, 2019) advocates for *simple and already interpretable* models. Indeed, for various real-world problems, simple interpretable models perform similarly to more complex models (Semenova et al., 2019) and should therefore be preferred.

Unfortunately, this solution is not applicable for high-dimensional and/or complex problems where the representational capabilities of end-to-end deep learning models give them an edge against other models, e.g. autonomous driving (Gupta et al., 2021) or machine translation (Wu et al., 2016). In these cases, interpretability can be achieved in two ways. *Post-hoc* methods, such as feature attribution methods (Ancona et al., 2018), can be leveraged to produce an explanation for a model that *has already been trained*. Alternatively, it is possible to directly train complex *ante-hoc* models, which are models with some kind of “in-built mechanism” that allows for their scrutiny. Classical examples are decision trees (Quinlan, 1986). Recently, there has been an increased interest in developing ante-hoc deep learning models that attempt at retaining the representational and generalization properties of neural networks, whilst still being interpretable (e.g. Chen et al., 2019; Alvarez Melis and Jaakkola, 2018; Nguyen and Martínez, 2019).

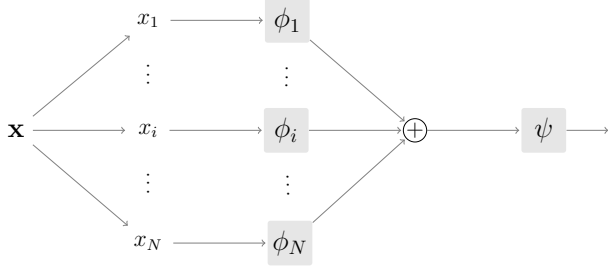


Figure 1: The Base Architecture of FLANs. A sample \mathbf{x} is split in its features x_i . Each of the feature is fed to a different function ϕ_i . All the processed features are then aggregated by summation, and finally fed to a prediction network ψ . In our work, all the functions ϕ_i and ψ are implemented as neural networks.

In this paper, we introduce a model, which we denominate *FLAN* (Feature-wise Latent Additive Network), that belongs to this last class of interpretable models. Inspired by linear models, FLAN computes a latent representation of each feature (or subsets thereof) *separately*. The latent representation of an input sample is obtained by simply *summing* the feature representations, and then passed to a classifier network for classification. We posit that these two constraints are what enables the interpretability of our model (Section 2.1). Despite these constraints, our model can still achieve good performance on a series of benchmark tasks in different domains.

2 FLANs

2.1 Interpretability Lessons from Linear Models

Linear models are generally considered among the prime examples of interpretable models. Arguably this is due to two key characteristics of these models:

- *Separability of features*: Linear models do not take *interactions* among features into account (unless an interaction term is explicitly added to the features). This means that a user can examine the effect of each feature *separately* from the others. This, in turn, makes the model easier to understand from a user perspective (Schulz et al., 2017)
- *Predictability of the output*: Given a single feature, its effect on the output can be easily understood by a human user if the relationship is linear (Byun, 1995). In the presence of multiple features, the human can still easily predict their effect on the output(s), if their effect is separable as discussed in the previous point.

2.2 Model Architecture

Motivated by the previous section, we want to build a model for which the effect of single features can be predicted separately from each other. Let us assume that our goal is to learn a function $f : \mathcal{X} \rightarrow \mathcal{Y}$, where \mathcal{X} has dimension N and \mathcal{Y} has dimension M . We propose to implement the function f as:

$$f(\mathbf{x}) = f(x_1, \dots, x_i, \dots, x_N) = \psi\left(\sum_{i=1}^N \phi_i(x_i)\right) \quad (1)$$

where:

- x_i (with $i = 1, \dots, N$) are the features, i.e. the components of the input sample \mathbf{x} ;
- $\phi_i : \mathcal{X}_i \rightarrow \mathcal{Z}$ are feature functions that act on each individual feature x_i separately and map them to the *same* latent space \mathcal{Z} of dimension D . Note that the feature functions may either implement different functions, or the same function for all features;
- the aggregate $\sum_{i=1}^N \phi_i(x_i) = \mathbf{z} \in \mathcal{Z}$ is the latent representation for the input sample \mathbf{x} ;
- the predictor function $\psi : \mathcal{Z} \rightarrow \mathcal{Y}$ maps the sample latent representation to the output space \mathcal{Y} .

In this paper, we implement the feature functions ϕ_i and the prediction function ψ as neural networks and learn them in an end-to-end fashion. Figure 1 provides a depiction of our model.

Before discussing the interpretability of our model (Section 2.3), we would like to make a few remarks.

Remark 2.2.1 (Universal Approximation). Since no interaction is explicitly modeled in Eq. (1), a concern that may be raised is if our model still retains the same approximation capabilities of traditional neural networks. The answer is given by the *Kolmogorov-Arnold representation theorem* (Kolmogorov, 1957) which claims, informally, that any continuous function of a finite number of variables can be expressed in the form

$$f(\mathbf{x}) = f(x_1, \dots, x_N) = \sum_{q=0}^{2N} \Phi_q\left(\sum_{i=1}^N \phi_{q,i}(x_i)\right)$$

Note that for interpretability purposes, we do not need the outer sum since it would not separate neither the outputs nor the effects of the input features. We therefore use a more generic function ψ . The strength of the Kolmogorov-Arnold representation theorem is in claiming that there is actually *no need* to explicitly model

interactions. Although there is some debate about the applicability of the Kolmogorov-Arnold theorem (e.g. Girosi and Poggio, 1989; Kůrková, 1991), in Section 4 we experimentally show that our model can (over)fit the training dataset.

Remark 2.2.2 (Feature Subgroups). In some applications, having a function applied to each individual feature may be detrimental. From an interpretability perspective, this is especially true when a single feature has no particular meaning. For example, consider computer vision tasks: human users rarely understand image classification in terms of single pixels, but rather in terms of higher-level concepts. Eq. (1) can be adapted to consider features in (*non-overlapping*) groups rather than individually. Building on the computer vision example, an image could be processed in *patches* rather than single pixels.

Remark 2.2.3 (Structural Information). Some data types carry additional structural information, e.g. natural language or images. Eq. (1) can be applied directly also to these domains. However, for the purpose of parameter sharing, it may be useful to make the dependency on the structure explicit:

$$f(\mathbf{x}) = f(x_1, \dots, x_N) = \psi\left(\sum_{i=1}^N \phi(x_i; \theta, p_i)\right)$$

where θ are parameters common to all the feature functions, and p_i encode some kind of structural information. This is the same idea behind the positional embeddings used in Transformer architectures (Vaswani et al., 2017).

2.3 Interpreting FLANs

In this section, we will discuss the three main modalities to interpret FLANs. Concrete examples will then be presented in Section 4.

2.3.1 Separating and Predicting the Affect of Individual Features

The interpretability of FLANs stems from the fact that different features are processed *separately*. That is, we can analyze how each feature contributes to the prediction without being concerned about interactions.

A user can study the effect of a single feature x_i simply by performing a prediction on that feature, i.e. $\psi(\mathbf{z}_i)$ with $\mathbf{z}_i = \phi_i(x_i)$. Note however that, since we are not making any assumption on the function ψ , the effect is not generally additive. In fact, assume that \mathcal{Y} and \mathcal{Z} are equipped, respectively, with norms $\|\cdot\|_{\mathcal{Y}}$ and $\|\cdot\|_{\mathcal{Z}}$. Further, let us informally assume that we can compute the Taylor expansion of ψ in a “large enough”

neighborhood of $\mathbf{z}_* = \sum_{j=1, j \neq i}^N \mathbf{z}_j$. Then we have

$$\underbrace{\|\psi(\mathbf{z}_* + \mathbf{z}_i) - \psi(\mathbf{z}_*) - \psi(\mathbf{z}_i)\|_{\mathcal{Y}}}_{(\Delta)} = \|\mathbf{J}_{\mathbf{z}_*} \mathbf{z}_i - \psi(\mathbf{z}_i) + o(\|\mathbf{z}_*\|_{\mathcal{Z}})\|_{\mathcal{Y}} \quad (2)$$

where:

- $\psi(\mathbf{z}_* + \mathbf{z}_i) - \psi(\mathbf{z}_*)$ is the change in prediction given by the additional information contained in the i -th feature;
- $\mathbf{J}_{\mathbf{z}_*}$ is the Jacobian of ψ computed at point \mathbf{z}_* ;
- $o(\|\mathbf{z}_*\|_{\mathcal{Z}})$ is the remainder term in the first-order Taylor expansion.

The right-hand side of Eq. (2) gets closer to zero the “more linear” is ψ . Therefore Eq. (2) is telling us that we can estimate the change in prediction (Δ) given by feature i by looking at the prediction $\psi(\mathbf{z}_i)$ on that feature. The accuracy of the estimation will depend on how non-linear is ψ . Although, we are not making any assumption on ψ , in Section 4.2 we show that in practice we can still estimate the effect of single features on the prediction.

2.3.2 Feature Importance

The interpretability modality described in the previous section has mostly an “algorithmic/mechanistic” flavor. However, FLANs can be interpreted also by computing feature importances without the need for *post-hoc* methods, such as SHAP (Lundberg and Lee, 2017). Since sample representations are simply the *sum* of feature representations, then a feature i that is mapped to a small vector $\|\mathbf{z}_i\|_{\mathcal{Z}} \approx 0$ brings no contribution to the prediction. This means that we can use the norms of the feature latent representations as indicative of feature importance.

2.3.3 Example-Based

FLANs can be further interpreted via examples/prototypes: to interpret the model at an input sample $\hat{\mathbf{z}}$, we only need to look for the nearest samples $\bar{\mathbf{z}}$ in the latent space. Since ψ in our model is a neural network, and therefore a Lipschitz continuous function, i.e. $\|\psi(\hat{\mathbf{z}}) - \psi(\bar{\mathbf{z}})\|_{\mathcal{Y}} \leq L\|\hat{\mathbf{z}} - \bar{\mathbf{z}}\|_{\mathcal{Z}}$, the predictions performed on two samples with similar representations will be similar.

This analysis can be performed also on a feature level. That is, by looking for features with similar representations, we can understand which features provide similar information towards the prediction. Similarly, by looking at *dissimilar* features, we are able to understand why two samples may be classified differently.

3 RELATED WORK

Our work is motivated by interpretability. In the taxonomy (Molnar, 2019) of interpretability methods, FLANs classifies primarily as a *local* method since the model can be explained at single sample points. A more *global* overview of the model can be obtained by looking for similar samples in the latent space, as explained in Section 2.3.3. Here, any of previously proposed methods can be used (e.g. MMD-Critic by Kim et al. 2016, ProtoDash by Gurumoorthy et al. 2017).

FLANs can be inspected also via feature attributions (Section 2.3.2). These feature importances are computed as norms of the feature representations. Therefore there is no need to use any post-hoc method, such as gradient-based methods (Ancona et al., 2018; Selvaraju et al., 2017; Bhatt et al., 2019; Sundararajan et al., 2017) or SHAP (Lundberg and Lee, 2017), which would require more computational resources. This advantage is shared with Transformer models (Vaswani et al., 2017), where the attention scores can be interpreted as importances. However, the attention scores are function of *all* the feature, effectively modeling interactions. This, in turn, decreases separability and, consequently, interpretability.

From a modeling perspective, FLANs belong to the class of *ante-hoc structurally constrained* deep learning models. Notable methods in this category are those that augment the network with prototype/prototypical-part based reasoning, e.g. (Li et al., 2017; Chen et al., 2019). A similar mechanism can be achieved also with FLANs (Section 2.3.3) without the need of an *ad-hoc* cost function or training strategy. Prototypes are similar in spirit to the concepts/feature basis used in Self-Explaining Neural Networks (SENNs) (Alvarez Melis and Jaakkola, 2018). Interestingly, (Alvarez Melis and Jaakkola, 2018) also recognize the value of additivity/separability for interpretability. However, additivity is enforced only in the last layer in their model. The concepts (and their relevances) are computed as functions of the entire input space. Consequently, the interpretability with respect to the original input space is lost.

Closer in spirit to our model are the neural additive models (Agarwal et al., 2020), Explainable Boosting Machines (EBM) (Nori et al., 2019), and the generalized additive models with interactions (Lou et al., 2013). However, these previous works do not leverage a second prediction function after aggregating the per-feature functions, thus potentially losing the approximation capabilities of FLANs. Moreover, the authors demonstrate their model only on tabular datasets, while we show that additivity-based models can be successfully used also in other more complex domains.

4 EXPERIMENTAL RESULTS

4.1 FLAN Benchmarking Results

Datasets. We test FLANs on a series of benchmark datasets across different domains. In the tabular domain, we consider ProPublica’s Recidivism Risk score prediction dataset (COMPAS)¹, and different risk datasets from the UCI benchmark repository (Dua and Graff, 2017) (`heart`, `adult`, `mammo`). For image classification, we benchmark FLANs on the two standard digit classification datasets MNIST (LeCun et al., 1998) and SVHN (Netzer et al., 2011), and the fine-grained bird recognition task CUB-200-2011 (Welinder et al., 2010). For text datasets, we consider AGNews (Zhang et al., 2015) and IMDb (Maas et al., 2011). For the textual domain, we further consider the healthcare-oriented TCR-Epitope dataset, where the task is to predict two amino-acid sequences will bind (binary classification). We refer to Weber et al. (2021) for more details. The results are summarised in Table 1.

Models for Comparison and Training. We compare FLANs to both established and state-of-the-art methods. The chosen models for each domain are reported in Table 1. For tabular datasets, we train all the models ourselves. For the other tasks, we only train FLANs and retrieve the performance of other models from the literature. Training details (Appendix 6) and further results (Appendix 8) are provided in the appendix. However, it is important to specify how FLANs splits the features in each task. For tabular tasks, FLANs simply process each feature individually. Similarly, in text datasets, our model considers each token (i.e. either a word for AGNews and IMDb, or a single amino-acid for TCR-Epitope) in the sentence/sequence as a single feature. For image datasets, *non-overlapping* square patches are the features fed to FLANs (Remark 2.2.2).

Tabular Datasets Results. For benchmarking on tabular datasets, we follow Agarwal et al. (2020) and measure the performance of different models in terms of Area Under the Curve (AUC). Table 1a shows that these datasets are easy enough that a simple logistic regression model can perform well. The results on the `adult` and `mammo` datasets suggest that linearity is a good inductive bias for these tasks since logistic regression is able to consistently outperform all the other (non-linear) models. On the other hand, in the `heart` dataset and, to a lesser degree, in the COMPAS dataset, it seems beneficial to include non-linearities and interactions. In particular, FLANs closely replicates the performance of more traditional feedforward networks

¹<https://github.com/propublica/compas-analysis/>

(MLP). This might suggest that FLANs are similar to MLPs in terms of approximation capabilities.

Image Datasets Results. FLANs results (Table 1b) on the MNIST dataset are comparable to established methods. Moreover, linear models (results not reported) do not achieve more than 94% test accuracy, providing further evidence to the ability of FLANs in implementing interactions *without explicitly modeling them*. We further tested our model on the more difficult fine-grained image classification dataset CUB-200-2011. FLANs do not achieve the same accuracy as other models. This might be explained by the fact that the models reported are pretrained on ImageNet (Russakovsky et al., 2014) and further finetuned on this dataset. On the other hand, in our experiments, our top-performing models use only *some layers* of a pretrained ResNeXt (Xie et al., 2017) as part of the patch feature function ϕ_i . We hypothesize that the inferior performance of FLANs is attributed to the fact that our model has to essentially *learn the interactions from scratch*, and CUB-200-2011 might be a too small of a dataset to effectively learn this. Despite the lower accuracy, and given the relatively small size of the dataset (11.7k images split across 200 classes), we see our results as promising and a good basis for future investigations in *large scale* image recognition tasks that require interpretability.

Text Datasets Results. On the considered benchmark datasets, FLANs fair well against traditional LSTM/CNN-based models. The drop in performance of FLANs is particularly noticeable on the IMDB against more modern attention-based architectures. Considering that IMDB contains much longer sentences than AGNews, these results suggest that FLANs may have difficulties in learning longer term dependencies/interactions. This is consistent with the conclusion reached on image datasets.

TCR-Epitope Dataset Results. FLAN outperforms the K-Nearest Neighbor baselines by a large margin and achieves comparable results to TITAN (Weber et al., 2021), the state-of-the-art deep model for the task, *even without pretraining or augmentation strategies*.

Summary. FLANs managed to achieve results comparable to the most established models on a series of benchmark datasets. Results against more recent architectures suggest that FLANs may have difficulties in learning complex/long interactions. However, it is worth noting that FLANs do manage to achieve 100% training accuracy in our experiments (Appendix 8). This suggests that our model is able to learn complex interactions, although they may not be *generalizable*.

Table 1: Benchmarking Results. (*) denotes pretrained models or models using automated augmentation strategies (e.g. Cubuk et al., 2020). (**) denotes FLAN models that use pretrained models as *part* of the feature functions.

(a) Area Under The Curve (AUC) on Tabular Datasets.

	COMPAS	adult	heart	mammo
Logistic Regression	0.905	0.892	0.873	0.841
Decision Tree (small)	0.903	0.865	0.849	0.799
Decision Tree (unrestricted)	0.902	0.813	0.848	0.801
Random Forest	0.915	0.869	0.945	0.822
EBM (Nori et al., 2019)	0.911	0.893	0.941	0.840
MLP	0.915	0.874	0.937	0.831
SENN (Alvarez Melis and Jaakkola, 2018)	0.910	0.865	0.881	0.834
FLAN	0.914	0.880	0.950	0.832

(b) Test Accuracy (%) on Image Datasets.

	MNIST	SVHN	CUB
ResNet (He et al., 2016; Wang et al., 2020)	99.2	94.5*	84.5*
iCaps (Wang et al., 2020)	99.2	92.0	-
ViT (Dosovitskiy et al., 2021; He et al., 2021)	-	88.9	90.4*
ProtoPNet (Chen et al., 2019)	-	-	84.8*
SENN (Alvarez Melis and Jaakkola, 2018)	99.1	-	-
SotA (Byerly et al., 2020; Cubuk et al., 2020)	99.84	99.0*	91.3*
FLAN	99.05	93.41	71.53**

(c) Test Accuracy (%) on Text Datasets.

	AGNews	IMDb
CharCNN (Zhang et al., 2015)	90.49	-
LSTM (Wang, 2018; Dai and Le, 2015)	93.8	86.5
VDCNN (Conneau et al., 2017; Abreu et al., 2019)	91.33	79.47
HAHNN (Abreu et al., 2019)	-	95.17
XLNet (Yang et al., 2019)	95.6*	96.8*
FLAN	91.2	85.2

(d) AUC on the TCR-Epitope Dataset.

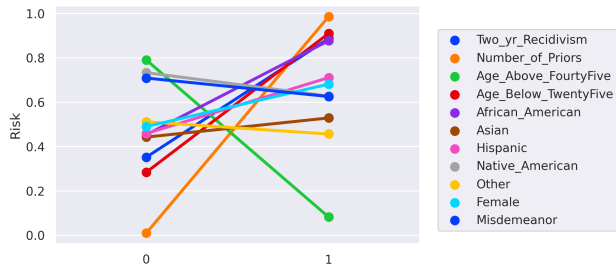
	TCR-Epitope
KNN ($K = 7$)	0.770
KNN ($K = 21$)	0.779
TITAN Weber et al. (2021)	0.841
Augmented TITAN (Weber et al., 2021)	0.867*
FLAN	0.858

4.2 Interpretability Results

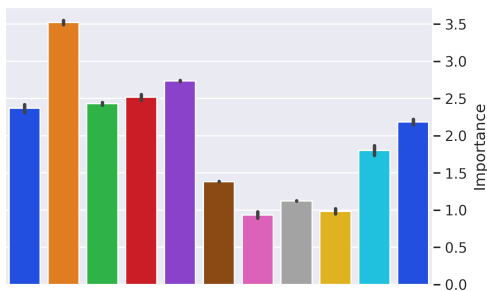
4.2.1 COMPAS

We use the COMPAS dataset as a propedeutic example to show how to interpret FLANs. As discussed in Section 2.3.1, we can study the approximate effect of single features separately, by applying the prediction network ψ to the feature latent representation. In this case study, this is even easier since all the features are binarized. Figura 2a shows how the predicted risk changes if we switch a feature from 0 to 1. The results suggest that the risk is *increased* for criminals that have a high number of priors, are younger than 25, are Afro-American, or have already re-offended in the past two years. Interestingly, the risk seems particularly

decreased for criminals above the age of 45. To further validate these findings we analyze the feature importances provided by our model. For each sample, we compute the importances as explained in Section 2.3.2 and then we average them over the training set. Figure 2b confirms that across the training set, the features mentioned above are the most discriminative ones. Previous analyses performed using interpretable models (Agarwal et al., 2020; Alvarez Melis and Jaakkola, 2018) reached similar conclusions.



(a) Feature Effects



(b) Feature Importances

Figure 2: Interpreting A FLAN Model Trained On The COMPAS Dataset. (a) Effect of the single features. (b) Feature importances averaged over the training set. The legend in the center shows the colors used to denote each feature.

4.2.2 CUB

We qualitatively validate the interpretability capabilities of our model on the more complex CUB-200-2011 dataset. For further qualitative results, please refer to Appendix 8.

Feature Importances. We start by comparing the feature importances natively provided by FLANs against three gradient-based *post-hoc* feature attribution methods: Integrated Gradients (Sundararajan et al., 2017), Saliency (Simonyan et al., 2013), and InputXGradient (Kindermans et al., 2016). Figure 3 shows the importances computed by the aforementioned methods for a test sample correctly predicted as a **Black Footed Albatross**. The norms of the la-

tent representations (Section 2.3.2) highlight features that are typically used to identify birds, i.e. the region around the eye and the beak (Chen et al., 2019). While noisier, gradient-based methods highlight some of the same regions, partially validating our model. However, IntegratedGradients and Saliency also highlight some areas in the top-right part of the image. In the next paragraph, we argue that these regions might be indicative of *counterfactual* evidence, rather than “direct” evidence.

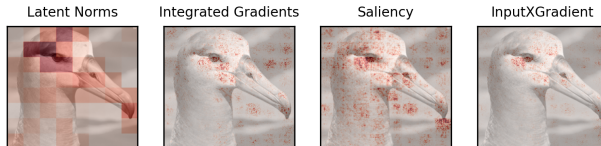


Figure 3: Comparison of the feature importances computed by our model (Latent Norms) against 3 established gradient-based feature attribution methods.

Algorithmic Interpretation. To show that the top-right area of the image is not particularly important towards the prediction of the sample at hand, we leverage the algorithmic interpretation modality described in Section 2.3.1. More precisely, we drop from the inner sum of Eq. (1) those features with the smallest latent norm. This is shown in Figure 4 (left). Note that this is different from occluding the image (Zeiler and Fergus, 2014). As shown at the top of Figure 4 (left), the incomplete image is still classified as **Black Footed Albatross**. This makes sense since, as argued in Section 2.3.2, features with small norm do not contribute to the sample representation and, consequently, to the prediction. This confirms that the top-right area is not important as direct evidence towards **Black Footed Albatross**. Rather it may be an area that, if modified, it may *become* important towards a different classification, i.e. a counterfactual.

To further demonstrate the usefulness of separability towards interpretability, we note that the incomplete image has a 10% chance to be classified as **Black Billed Cuckoo**. To see why it may be, we can apply the prediction network on the single patches. The 3 rightmost images in Figure 4 show how the top 3 patches are classified. In particular, we note that the first and third patch provide evidence towards **Black Billed Cuckoo**.

Example-Based Explanations. We finally show the third modality for interpreting FLANs, i.e. by examples. As discussed in Section 2.3.3, to do this we need to look for the nearest neighbors in the latent space \mathcal{Z} before the prediction network. While it can be argued that any layer in the prediction network can be used

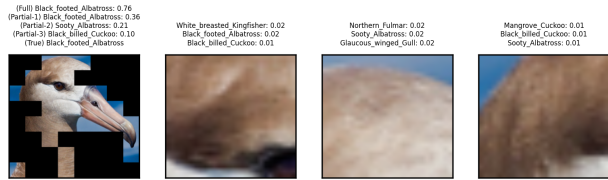


Figure 4: Algorithmic Interpretation of FLANs. In the leftmost image, we show the top 20 most important patches for a **Black Footed Albatross**. On top of the image we report the top 3 predicted classes (with probabilities) computed on the shown partial image. For reference, we provide also the prediction on the full image and the true label. In the 3 rightmost images we show the top 3 most important patches, together with the top 3 predictions for each of them.

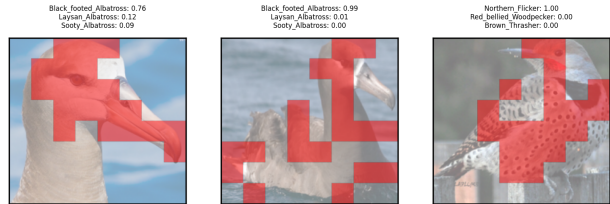


Figure 5: Example-Based Interpretation of FLANs. (Left) Reference image. (Center) Closest image in the latent space. (Right) Farthest image in the latent space. Above each image, we report the top 3 predicted classes (with probabilities). We highlight in red the patches that explain *why* the center (resp. right) image is close (resp. far) from the reference image.

4.3 Quantitative interpretability evaluation

as a sample representation for nearest neighbor search, we argue that the representation before the prediction network is the most representative of the sample. This is because this is the first point where the information from all the features is aggregated, and no further processing has been performed yet (cf. data processing inequality, e.g. Cover and Thomas 2006). Figure 5 shows the bird (center) that most closely resembles the reference **Black Footed Albatross** (left). In particular, for these images, the top 3 classes predicted are the same (reported on top of the images). However, it can be noted that the computed probabilities for each of these classes are different for the two birds. This means that the two images contain somewhat different information. It is then reasonable to wonder what information do the two images have in common, i.e. why are these two images similar/different? This can be an important question for assessing similarity models (Eberle et al., 2020). With FLANs, this question can be answered by means of a *linear assignment problem* (Burkard and Çela, 1999). More details are provided in Appendix 7.

The red patches in the central image of Figure 5 are the *most similar* patches assigned to the top features of the reference image on the left. These results show that, again, the eyes of a bird are a distinctive feature. In particular, this feature seems to drive the similarity between the two images. Analogously, if we look for the *most dissimilar* patches between the reference image and the most dissimilar training sample (rightmost image in Figure 5), we find that the eyes (together with the feathers) are used to distinguish the **Black Footed Albatross** from the **Northern Flicker**.

Quantitatively assessing a subjective matter, such as interpretability, can be cumbersome. One of the ways for this quantitative evaluation is what Doshi-Velez and Kim (2017) call *functionally-grounded* evaluation. In particular, we leverage the recent work by Nguyen and Martínez (2020), where the authors propose a series of metrics to assess the *faithfulness* of an explanation (i.e. how “correct” is the explanation) and its broadness (i.e. how general it is).

For feature attributions, the faithfulness is partially assessed by *monotonicity* (computed as how unpredictable the sample becomes if important features are removed) and by *non-sensitivity* (i.e. unimportant features should not be given a high score). For example-based methods, faithfulness is given by the (inverse) *non-representativeness*, where representativeness means that the similar samples should be classified similarly. Broadness, instead, is given by the *diversity* of the examples.

In Table 2, we compare the attribution scores natively provided by FLAN as the norms of the feature latent representations against the same methods mentioned in Section 4.2.2. In Table 3, we use the example-based metrics to evaluate if the feature latent space (LS) is better than the original input space (OS) for the selection of (12) prototypes via K-Medoids (Kaufman and Rousseeuw, 2009). The same analysis can be done using a different method such as ProtoDash (Gurumoorthy et al., 2017). Note that we evaluate example-based strategies in both a local and global setting. In the global, we select examples to explain whole classes, while in the local we want to explain individual test samples using their nearest training samples.

The non-sensitivity results show that FLAN tends to either assign some importance to not influential features, or no importance to influential features. This can be

Table 2: Comparison of FLAN norms, Integrated Gradients (IG), InputXGradient (InpXGrad), and Saliency using feature attribution metrics.

(a) Monotonicity. Higher is better.						(b) Non-Sensitivity. Lower is better.					
	TCR-Epitope	MNIST	CUB	SVHN	AGNews		TCR-Epitope	MNIST	CUB	SVHN	AGNews
FLAN	0.17	0.10	0.02	0.04	0.17	FLAN	52.89	483	1886.00	27.29	11.70
IG	0.07	0.15	0.03	0.04	0.16	IG	25.19	1.83	5.40	4.57	12.58
InpXGrad	0.07	0.16	0.04	0.03	0.15	InpXGrad	24.04	3.50	5.80	5.14	10.59
Saliency	0.10	0.15	0.06	0.04	0.09	Saliency	23.50	168.85	111501.20	1015.44	42.19

Table 3: Comparison of examples/prototypes computed by clustering in the Original input Space (OS) and the feature Latent Space (LS) in both the local and global setting. Comparison by diversity (D, higher is better) and non-representativeness (NR, lower is better).

	TCR-Epitope		MNIST		CUB		SVHN		AGNews	
	OS	LS	OS	LS	OS	LS	OS	LS	OS	LS
Local D	299.27	51.85	68.35	66.09	1507.18	1187.72	67.23	203.82	0.51	0.53
Local NR	2.21	2.39	2.15	2.19	3.63	3.47	2.14	2.13	0.87	0.10
Global D	671.46	67.74	61.01	60.49	1376.06	1332.07	185.15	190.12	0.31	0.48
Global NR	0.18	0.25	2.16	2.17	3.81	3.83	2.09	2.09	7e-3	6e-4

explained if we note that the reported non-sensitivity is particularly unfavorable for patch-based FLANs in image classification: to make the attribution methods comparable we needed an attribution scores for *each pixel*, and therefore for FLAN scores we assigned the same value to each pixel in a given patch, even though certain pixels may not actually have any influence. This also explains the relatively low, but comparable monotonicity performance of FLAN scores on the image datasets. However, in non-patch-based datasets, FLAN scores seem to perform best. Considering the above points, overall FLAN performs satisfactorily, showing that to FLANs interpret via attribution analysis there is *no need to rely on post-hoc methods*.

The example-based metrics (Table 3) show that there does not seem to be a clear advantage between clustering in the original input space or in the latent space, apart for more extreme cases (e.g. TCR-Epitope and SVHN). This suggests that an user may simply apply example-based strategies directly to the input space. However, we argue that example-based analysis in the feature space may turn out useful in two instances. Firstly, FLAN feature spaces offer the possibility to identify which features drive the (dis-)similarity of the selected prototypes (Section 4.2.2). Secondly, sometimes using the euclidean distance in the feature space may reveal easier than either defining or computing a distance in the original input space (e.g. when dealing with graphs), therefore offering a computational advantage.

5 CONCLUSION

In this paper, we introduced a class of *powerful and interpretable* models, which we call FLANs. In terms of prediction accuracy, our results show that our model can achieve reasonable performance on *complex datasets*. We demonstrate how our model can be easily and natively interpreted *without the need of post-hoc methods* and *without major drawbacks in terms of interpretability* (according to recently introduced metrics).

We believe that our work represents an important contribution towards interpretable machine learning in *complex domains* with profound societal impact, e.g. histopathology and healthcare. In future work, we plan to address the generalization difficulties of our model. Moreover, we plan to run user studies to further validate the interpretability of our model.

Acknowledgements

We acknowledge funding by the European Union’s Horizon 2020 research and innovation programme (iPC–Pediatric Cure, No. 826121).

References

G. Cybenko. Approximation by superpositions of a sigmoidal function. *Mathematics of Control, Signals, and Systems*, 2(4):303–314, 12 1989. ISSN 09324194. doi: 10.1007/BF02551274. URL <https://link.springer.com/article/10.1007/BF02551274>.

- Kurt Hornik, Maxwell Stinchcombe, and Halbert White. Multilayer feedforward networks are universal approximators. *Neural Networks*, 2(5):359–366, 1 1989. ISSN 08936080. doi: 10.1016/0893-6080(89)90020-8.
- Kenji Kawaguchi, Leslie Pack Kaelbling, and Yoshua Bengio. Generalization in Deep Learning. *arXiv*, 10 2017. URL <http://arxiv.org/abs/1710.05468>.
- Sanjeev Arora, Rong Ge, Behnam Neyshabur, and Yi Zhang. Stronger generalization bounds for deep nets via a compression approach. In *35th International Conference on Machine Learning, ICML 2018*, pages 390–418, 2018.
- Cynthia Rudin. Stop explaining black box machine learning models for high stakes decisions and use interpretable models instead. *Nature Machine Intelligence*, 1(5):206–215, 5 2019. doi: 10.1038/s42256-019-0048-x.
- Lesia Semenova, Cynthia Rudin, and Ronald Parr. A study in Rashomon curves and volumes: A new perspective on generalization and model simplicity in machine learning. *arXiv*, 8 2019. URL <http://arxiv.org/abs/1908.01755>.
- Abhishek Gupta, Alagan Anpalagan, Ling Guan, and Ahmed Shaharyar Khwaja. Deep learning for object detection and scene perception in self-driving cars: Survey, challenges, and open issues. *Array*, 10:100057, 7 2021. ISSN 25900056. doi: 10.1016/j.array.2021.100057.
- Yonghui Wu, Mike Schuster, Zhifeng Chen, Quoc V. Le, Mohammad Norouzi, Wolfgang Macherey, Maxim Krikun, Yuan Cao, Qin Gao, Klaus Macherey, Jeff Klingner, Apurva Shah, Melvin Johnson, Xiaobing Liu, Łukasz Kaiser, Stephan Gouws, Yoshikiyo Kato, Taku Kudo, Hideto Kazawa, Keith Stevens, George Kurian, Nishant Patil, Wei Wang, Cliff Young, Jason Smith, Jason Riesa, Alex Rudnick, Oriol Vinyals, Greg Corrado, Macduff Hughes, and Jeffrey Dean. Google’s Neural Machine Translation System: Bridging the Gap between Human and Machine Translation. 9 2016. URL <http://arxiv.org/abs/1609.08144>.
- Marco Ancona, Enea Ceolini, Cengiz Oztireli, and Markus Gross. Towards better understanding of gradient-based attribution methods for Deep Neural Networks. In *6th International Conference on Learning Representations (ICLR 2018)*, 2018.
- J. R. Quinlan. Induction of decision trees. *Machine Learning*, 1(1):81–106, 3 1986. ISSN 0885-6125. doi: 10.1007/bf00116251. URL <https://link.springer.com/article/10.1007/BF00116251>.
- Chaofan Chen, Oscar Li, Daniel Tao, Alina Barnett, Cynthia Rudin, and Jonathan K Su. This Looks Like That: Deep Learning for Interpretable Image Recognition. In H Wallach, H Larochelle, A Beygelzimer, F d Alché-Buc, E Fox, and R Garnett, editors, *Advances in Neural Information Processing Systems 32*, pages 8930–8941. Curran Associates, Inc., 2019. URL <http://papers.nips.cc/paper/9095-this-looks-like-that-deep-learning-for-interpretability.pdf>.
- David Alvarez Melis and Tommi Jaakkola. Towards Robust Interpretability with Self-Explaining Neural Networks. In S Bengio, H Wallach, H Larochelle, K Grauman, N Cesa-Bianchi, and R Garnett, editors, *Advances in Neural Information Processing Systems 31*, pages 7775–7784. Curran Associates, Inc., 2018. URL <http://papers.nips.cc/paper/8003-towards-robust-interpretability-with-self-explaining.pdf>.
- A.-P. Nguyen and M.R. Martínez. MonoNet: Towards Interpretable Models by Learning Monotonic Features, 2019.
- Eric Schulz, Joshua B. Tenenbaum, David Duvenaud, Maarten Speekenbrink, and Samuel J. Gershman. Compositional inductive biases in function learning. *Cognitive Psychology*, 99:44–79, 12 2017. ISSN 00100285. doi: 10.1016/j.cogpsych.2017.11.002.
- Eunhee Byun. Interaction between prior knowledge and type of nonlinear relationship on function learning. *Theses and Dissertations Available from ProQuest*, 1 1995. URL <https://docs.lib.purdue.edu/dissertations/AAI9622674>.
- Andrei Nikolaevich Kolmogorov. On the representation of continuous functions of many variables by superposition of continuous functions of one variable and addition. In *Doklady Akademii Nauk*, volume 114, pages 953–956, 1957.
- Federico Girosi and Tomaso Poggio. Representation Properties of Networks: Kolmogorov’s Theorem Is Irrelevant. *Neural Computation*, 1(4):465–469, 12 1989. ISSN 0899-7667. doi: 10.1162/neco.1989.1.4.465.
- Věra Kůrková. Kolmogorov’s Theorem Is Relevant. *Neural Computation*, 3(4):617–622, 12 1991. ISSN 0899-7667. doi: 10.1162/neco.1991.3.4.617. URL <http://direct.mit.edu/neco/article-pdf/3/4/617/812230/neco.1991.3.4.617.pdf>.
- Ashish Vaswani, Noam Shazeer, Niki Parmar, Jakob Uszkoreit, Llion Jones, Aidan N. Gomez, Łukasz Kaiser, and Illia Polosukhin. Attention is all you need. In *Advances in Neural Information Processing Systems*, volume 2017-December, pages 5999–6009. Neural information processing systems foundation, 6 2017. URL <https://arxiv.org/abs/1706.03762v5>.

- Scott M Lundberg and Su-In Lee. A Unified Approach to Interpreting Model Predictions. In I Guyon, U V Luxburg, S Bengio, H Wallach, R Fergus, S Vishwanathan, and R Garnett, editors, *Advances in Neural Information Processing Systems 30*, pages 4765–4774. Curran Associates, Inc., 2017. URL <http://papers.nips.cc/paper/7062-a-unified-approach-to-interpreting-model-predictions.pdf>.
- Christoph Molnar. *Interpretable Machine Learning*. 2019.
- Been Kim, Rajiv Khanna, and Oluwasanmi O Koyejo. Examples are not enough, learn to criticize! Criticism for Interpretability. In D D Lee, M Sugiyama, U V Luxburg, I Guyon, and R Garnett, editors, *Advances in Neural Information Processing Systems 29*, pages 2280–2288. Curran Associates, Inc., 2016.
- Karthik S. Gurumoorthy, Amit Dhurandhar, Guillermo Cecchi, and Charu Aggarwal. Efficient Data Representation by Selecting Prototypes with Importance Weights. *Proceedings - IEEE International Conference on Data Mining, ICDM*, 2019–November:260–269, 7 2017. URL <http://arxiv.org/abs/1707.01212>.
- Ramprasaath R. Selvaraju, Michael Cogswell, Abhishek Das, Ramakrishna Vedantam, Devi Parikh, and Dhruv Batra. Grad-CAM: Visual Explanations from Deep Networks via Gradient-Based Localization. In *Proceedings of the IEEE International Conference on Computer Vision*, volume 2017–October, pages 618–626. Institute of Electrical and Electronics Engineers Inc., 12 2017. ISBN 9781538610329. doi: 10.1109/ICCV.2017.74.
- Umang Bhatt, Pradeep Ravikumar, and Jose M. F. Moura. Towards Aggregating Weighted Feature Contributions. *arXiv*, 1 2019. URL <http://arxiv.org/abs/1901.10040>.
- Mukund Sundararajan, Ankur Taly, and Qiqi Yan. Axiomatic Attribution for Deep Networks. In *Proceedings of the 34th International Conference on Machine Learning - Volume 70, ICML'17*, pages 3319–3328. JMLR.org, 2017.
- Oscar Li, Hao Liu, Chaofan Chen, and Cynthia Rudin. Deep Learning for Case-Based Reasoning through Prototypes: A Neural Network that Explains Its Predictions. *32nd AAAI Conference on Artificial Intelligence, AAAI 2018*, pages 3530–3537, 10 2017. URL <http://arxiv.org/abs/1710.04806>.
- Rishabh Agarwal, Nicholas Frosst, Xuezhou Zhang, Rich Caruana, and Geoffrey E. Hinton. Neural Additive Models: Interpretable Machine Learning with Neural Nets. *arXiv*, 4 2020. URL <http://arxiv.org/abs/2004.13912>.
- Harsha Nori, Samuel Jenkins, Paul Koch, and Rich Caruana. InterpretML: A Unified Framework for Machine Learning Interpretability. 9 2019. URL <http://arxiv.org/abs/1909.09223>.
- Yin Lou, Rich Caruana, Johannes Gehrke, and Giles Hooker. Accurate intelligible models with pairwise interactions. In *Proceedings of the ACM SIGKDD International Conference on Knowledge Discovery and Data Mining*, volume Part F128815, pages 623–631. Association for Computing Machinery, 8 2013. ISBN 9781450321747. doi: 10.1145/2487575.2487579.
- Dheeru Dua and Casey Graff. UCI Machine Learning Repository, 2017. URL <http://archive.ics.uci.edu/ml>.
- Yann LeCun, Léon Bottou, Yoshua Bengio, and Patrick Haffner. Gradient-based learning applied to document recognition. *Proceedings of the IEEE*, 86(11): 2278–2323, 1998. ISSN 00189219. doi: 10.1109/5.726791.
- Yuval Netzer, Tao Wang, Adam Coates, Alessandro Bissacco, Bo Wu, and Andrew Y Ng. Reading digits in natural images with unsupervised feature learning. 2011.
- P Welinder, S Branson, T Mita, C Wah, F Schroff, S Belongie, and P Perona. Caltech-UCSD Birds 200. Technical Report CNS-TR-2010-001, California Institute of Technology, 2010.
- Xiang Zhang, Junbo Zhao, and Yann LeCun. Character-Level Convolutional Networks for Text Classification. In *Proceedings of the 28th International Conference on Neural Information Processing Systems - Volume 1, NIPS'15*, pages 649–657, Cambridge, MA, USA, 2015. MIT Press.
- Andrew L Maas, Raymond E Daly, Peter T Pham, Dan Huang, Andrew Y Ng, and Christopher Potts. Learning Word Vectors for Sentiment Analysis. In *Proceedings of the 49th Annual Meeting of the Association for Computational Linguistics: Human Language Technologies*, pages 142–150, Portland, Oregon, USA, 6 2011. Association for Computational Linguistics. URL <https://www.aclweb.org/anthology/P11-1015>.
- Anna Weber, Jannis Born, and María Rodríguez Martínez. TITAN: T-cell receptor specificity prediction with bimodal attention networks. *Bioinformatics*, 37(Supplement_1): i237–i244, 7 2021. ISSN 1367-4803. doi: 10.1093/BIOINFORMATICS/BTAB294. URL https://academic.oup.com/bioinformatics/article/37/Supplement_1/i237/6319659.
- Olga Russakovsky, Jia Deng, Hao Su, Jonathan Krause, Sanjeev Satheesh, Sean Ma, Zhiheng Huang, Andrej

- Karpathy, Aditya Khosla, Michael Bernstein, Alexander C. Berg, and Li Fei-Fei. ImageNet Large Scale Visual Recognition Challenge. *International Journal of Computer Vision*, 115(3):211–252, 9 2014. URL <http://arxiv.org/abs/1409.0575>.
- Saining Xie, Ross Girshick, Piotr Dollár, Zhuowen Tu, and Kaiming He. Aggregated residual transformations for deep neural networks. In *Proceedings of the IEEE conference on computer vision and pattern recognition*, pages 1492–1500, 2017.
- Ekin D Cubuk, Barret Zoph, Jonathon Shlens, and Quoc V Le. RandAugment: Practical Automated Data Augmentation with a Reduced Search Space. Technical report, 2020.
- Kaiming He, Xiangyu Zhang, Shaoqing Ren, and Jian Sun. Deep residual learning for image recognition. In *Proceedings of the IEEE Computer Society Conference on Computer Vision and Pattern Recognition*, volume 2016-December, pages 770–778. IEEE Computer Society, 12 2016. ISBN 9781467388504. doi: 10.1109/CVPR.2016.90. URL <http://image-net.org/challenges/LSVRC/2015/>.
- Zhengyang Wang, Xia Hu, and Shuiwang Ji. iCapsNets: Towards Interpretable Capsule Networks for Text Classification, 1 2020.
- Alexey Dosovitskiy, Lucas Beyer, Alexander Kolesnikov, Dirk Weissenborn, Xiaohua Zhai, Thomas Unterthiner, Mostafa Dehghani, Matthias Minderer, Georg Heigold, Sylvain Gelly, Jakob Uszkoreit, and Neil Houlsby. An Image is worth 16X16 words: Transformers for Image Recognition at Scale. In *ICLR*, 9 2021.
- Ju He, Jie-Neng Chen, Shuai Liu, Adam Kortylewski, Cheng Yang, Yutong Bai, Changhu Wang, and Alan Yuille. TransFG: A Transformer Architecture for Fine-grained Recognition. 3 2021. URL <http://arxiv.org/abs/2103.07976>.
- Adam Byerly, Tatiana Kalganova, and Ian Dear. A Branching and Merging Convolutional Network with Homogeneous Filter Capsules. 1 2020. URL <http://arxiv.org/abs/2001.09136>.
- Baoxin Wang. Disconnected recurrent neural networks for text categorization. In *ACL 2018 - 56th Annual Meeting of the Association for Computational Linguistics, Proceedings of the Conference (Long Papers)*, volume 1, pages 2311–2320. Association for Computational Linguistics (ACL), 2018. ISBN 9781948087322. doi: 10.18653/v1/p18-1215. URL <https://www.aclweb.org/anthology/P18-1215>.
- Andrew M. Dai and Quoc V. Le. Semi-supervised Sequence Learning. *Advances in Neural Information Processing Systems*, 2015-January:3079–3087, 11 2015. URL <http://arxiv.org/abs/1511.01432>.
- Alexis Conneau, Holger Schwenk, Yann Le Cun, and Loïc Barrault. Very Deep Convolutional Networks for Text Classification. Technical report, 2017. URL <https://www.aclweb.org/anthology/E17-1104>.
- Jader Abreu, Luis Fred, David Macêdo, and Cleber Zanchettin. Hierarchical Attentional Hybrid Neural Networks for Document Classification. In *Lecture Notes in Computer Science (including subseries Lecture Notes in Artificial Intelligence and Lecture Notes in Bioinformatics)*, volume 11731 LNCS, pages 396–402. Springer Verlag, 2019. ISBN 9783030304928. doi: 10.1007/978-3-030-30493-5{_}39.
- Zhilin Yang, Zihang Dai, Yiming Yang, Jaime Carbonell, Ruslan Salakhutdinov, and Quoc V. Le. XLNet: Generalized Autoregressive Pretraining for Language Understanding. *Advances in Neural Information Processing Systems*, 32, 6 2019. URL <http://arxiv.org/abs/1906.08237>.
- Karen Simonyan, Andrea Vedaldi, and Andrew Zisserman. Deep inside convolutional networks: Visualising image classification models and saliency maps. *arXiv preprint arXiv:1312.6034*, 2013.
- Pieter-Jan Kindermans, Kristof Schütt, Klaus-Robert Müller, and Sven Dähne. Investigating the influence of noise and distractors on the interpretation of neural networks. 11 2016. URL <http://arxiv.org/abs/1611.07270>.
- Matthew D. Zeiler and Rob Fergus. Visualizing and understanding convolutional networks. In *Lecture Notes in Computer Science (including subseries Lecture Notes in Artificial Intelligence and Lecture Notes in Bioinformatics)*, volume 8689 LNCS, pages 818–833. Springer Verlag, 11 2014. ISBN 9783319105895. doi: 10.1007/978-3-319-10590-1{_}53. URL <https://arxiv.org/abs/1311.2901v3>.
- Thomas M Cover and Joy A Thomas. *Elements of Information Theory (Wiley Series in Telecommunications and Signal Processing)*. Wiley-Interscience, USA, 2006. ISBN 0471241954.
- Oliver Eberle, Jochen Buttner, Florian Krautli, Klaus-Robert Müller, Matteo Valleriani, and Gregoire Montavon. Building and Interpreting Deep Similarity Models. *IEEE Transactions on Pattern Analysis and Machine Intelligence*, (01):1–1, 9 2020. ISSN 0162-8828. doi: 10.1109/tpami.2020.3020738.
- Rainer E. Burkard and Eranda Çela. Linear Assignment Problems and Extensions. In *Handbook of Combinatorial Optimization*, pages 75–149. Springer US, 1999. doi: 10.1007/978-1-4757-3023-4{_}2. URL https://link.springer.com/chapter/10.1007/978-1-4757-3023-4_2.

Finale Doshi-Velez and Been Kim. Towards a rigorous science of interpretable machine learning. *arXiv preprint arXiv:1702.08608*, 2017.

An-phi Nguyen and María Rodríguez Martínez. On quantitative aspects of model interpretability. *arXiv preprint arXiv:2007.07584*, 2020.

Leonard Kaufman and Peter J Rousseeuw. *Finding groups in data: an introduction to cluster analysis*, volume 344. John Wiley & Sons, 2009.

Diederik P. Kingma and Jimmy Lei Ba. Adam: A method for stochastic optimization. In *3rd International Conference on Learning Representations, ICLR 2015 - Conference Track Proceedings*. International Conference on Learning Representations, ICLR, 12 2015. URL <https://arxiv.org/abs/1412.6980v9>.

Ilya Loshchilov and Frank Hutter. Decoupled Weight Decay Regularization. *7th International Conference on Learning Representations, ICLR 2019*, 11 2017. URL <http://arxiv.org/abs/1711.05101>.

Liyuan Liu, Haoming Jiang, Pengcheng He, Weizhu Chen, Xiaodong Liu, Jianfeng Gao, and Jiawei Han. On the Variance of the Adaptive Learning Rate and Beyond. In *Proceedings of the Eighth International Conference on Learning Representations (ICLR 2020)*, 4 2020.

Ilya Loshchilov and Frank Hutter. SGDR: Stochastic Gradient Descent with Warm Restarts. *5th International Conference on Learning Representations, ICLR 2017 - Conference Track Proceedings*, 8 2016. URL <http://arxiv.org/abs/1608.03983>.

Supplementary Materials

6 Training details

All the deep learning models were trained using **Adam** (Kingma and Ba, 2015) (or variants thereof, i.e. **AdamW** Loshchilov and Hutter 2017, **RAdam** Liu et al. 2020). Learning rates varied in the set $\{0.001, 0.0005, 0.0001, 0.00005\}$. Training was tested with no learning rate scheduling, as well as exponential decay, step decay, and cosine annealing (Loshchilov and Hutter, 2016) (with and without restart). The chosen hyperparameters for each experiment can be retrieved from the corresponding `config.json` file provided in the accompanying code. Details about the architectures used are also provided in the accompanying code.

Tabular datasets. For each datasets, 10 different runs are performed. Table 1a reports means among these runs. In Table 4a we report again the mean, together with standard deviation and top performance (max).

Image datasets. For each datasets, 5 different runs are performed (with the best set of hyperparameters). Table 1b reports top performance among these runs. In Table 4b we report again the top performance (max), together with the mean among the 5 runs, and standard deviation.

Text datasets. For each datasets, 5 different runs are performed (with the best set of hyperparameters). Table 1c reports top performance among these runs. In Table 4c we report again the top performance (max), together with the mean among the 5 runs, and standard deviation.

TCR-epitope dataset. For this dataset 100 runs are performed (with the best set of hyperparameters). In a second setting, we add a pre-training step that learns the embedding representation separately for the TCR and epitope sequences. In this step, we utilize publicly available datasets containing only TCR or epitope sequences to find good representations and further improve FLAN’s ability to focus on meaningful positions/amino-acids. After pre-training, FLAN is implemented as usual. For this setting we once more performed 100 runs (with the best set of hyperparameters).

7 Detecting similar and different information content

While analyzing an example-based interpretation, we may wonder why two samples are similar/different. This can be answered relatively easily by leveraging the FLAN architecture. Informally, we can reformulate this question in the following way. Given the top K features of a sample \mathbf{x} , we would like to find the L features in the second sample $\hat{\mathbf{x}}$ that most closely match them. Mathematically,

$$\min_{S \subset \{1 \dots N\}, |S|=L} \left\| \sum_{i \in T} \mathbf{z}_i - \sum_{j \in S} \hat{\mathbf{z}}_j \right\| \quad (3)$$

where T (with $|T| = K$) is the set of the top K features \mathbf{z}_i of sample \mathbf{x} , and S is any subset of $\{1 \dots N\}$ of cardinality L . To simplify the problem, we restrict L to be equal to K . We further leverage the triangle inequality to split the norm of the sum in a sum of norms. We therefore end up with the following *linear assignment problem* (Burkard and Çela, 1999) with assignment function $A : T \rightarrow \{1, \dots, N\}$:

$$\min_A \sum_{i \in T} \|\mathbf{z}_i - \hat{\mathbf{z}}_{A(i)}\| \quad (4)$$

8 Further results

8.1 Performance results

Here we report more detailed performance results (Table 4). The experimental setup is reported in the previous section 6. Note that the inconsistencies in the results between Table 1 and Table 4 are due to the fact that new experiments have been run with *not* fixed random seeds to produce Table 4. However, this change does not affect the interpretation of the results discussed in Section 4.1.

Table 4: Further benchmarking results. (*) denotes pretrained models or models using automated augmentation strategies. (**) denotes FLAN models that use pretrained models as *part* of the feature functions. Reporting mean (max) \pm standard deviation over 10 runs for tabular datasets, and 5 runs for the other datasets.

(a) Area under the curve (AUC) on tabular datasets.

	COMPAS	adult	heart	mammo
Logistic Regression	0.905 (0.917) \pm 0.006	0.892 (0.896) \pm 0.003	0.873 (0.923) \pm 0.032	0.841 (0.874) \pm 0.017
Decision Tree (small)	0.903 (0.915) \pm 0.007	0.865 (0.871) \pm 0.005	0.849 (0.882) \pm 0.026	0.799 (0.818) \pm 0.017
Decision Tree (unrestricted)	0.902 (0.915) \pm 0.007	0.813 (0.821) \pm 0.005	0.848 (0.882) \pm 0.024	0.801 (0.826) \pm 0.016
Random Forest	0.915 (0.927) \pm 0.007	0.869 (0.877) \pm 0.004	0.945 (0.964) \pm 0.014	0.822 (0.841) \pm 0.016
EBM	0.911 (0.923) \pm 0.008	0.893 (0.896) \pm 0.002	0.941 (0.959) \pm 0.015	0.840 (0.869) \pm 0.015
MLP	0.915 (0.927) \pm 0.006	0.874 (0.883) \pm 0.005	0.937 (0.958) \pm 0.023	0.831 (0.856) \pm 0.014
SENN (Alvarez Melis and Jaakkola, 2018)	0.910 (0.922) \pm 0.007	0.865 (0.873) \pm 0.005	0.881 (0.925) \pm 0.036	0.834 (0.860) \pm 0.013
FLAN	0.914 (0.923) \pm 0.004	0.880 (0.886) \pm 0.004	0.950 (0.973) \pm 0.019	0.832 (0.867) \pm 0.019

(b) Test accuracy (%) on image datasets.

	MNIST	SVHN	CUB
ResNet	99.2	94.5*	84.5*
iCaps	99.2	92.0	-
ViT	-	88.9	90.4*
ProtoPNet	-	-	84.8*
SENN	99.1	-	-
SotA	99.84	99.0*	91.3*
FLAN	99.00 (99.05) \pm 0.0007	93.37 (93.41) \pm 0.0004	71.17 (71.53) \pm 0.003

(c) Test accuracy (%) on text datasets.

	AGNews	IMDb
CharCNN	90.49	-
LSTM	93.8	86.5
VDCNN	91.33	79.47
HAHNN	-	95.17
XLNet	95.6*	96.8*
FLAN	90.6 (90.9) \pm 0.003	84.9 (85.1) \pm 0.002

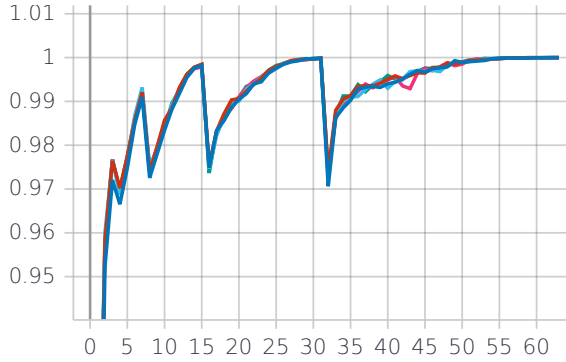
Table 5 summarizes the performance results for the two settings in the TCR-epitope dataset. Even though the performance metrics are almost identical, we argue that pretrained FLAN concentrates on more meaningful positions, since the amino-acid embedding representations are learned with more data.

Table 5: ROC-AUC and Balanced accuracy for FLAN and pretrained FLAN in the TCR-epitope dataset.

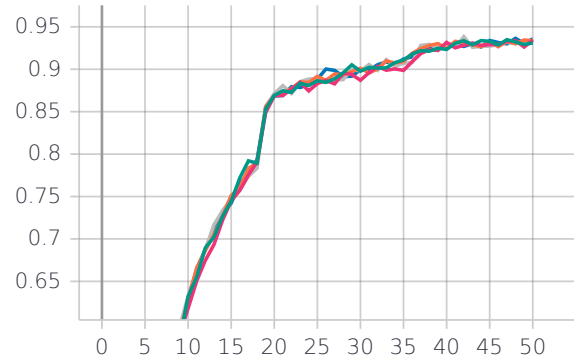
	AUC	B.Accuracy
FLAN	0,862 \pm 0,006	0,783 \pm 0,007
pretrained FLAN	0,858 \pm 0,004	0,780 \pm 0,006

8.1.1 Training graphs

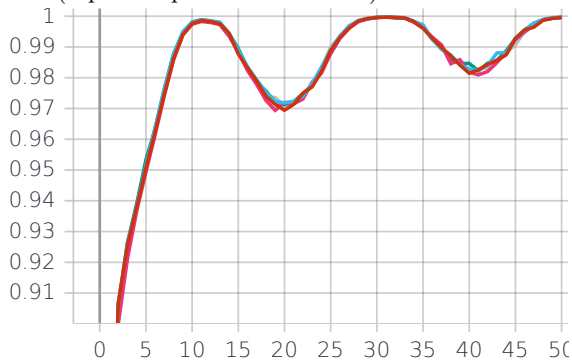
In Section 4.1 and Section 8.1 we reported the best models in terms of *test* performance. Here we report (Figure 6) the training curves of some models that achieved 100% (resp. 94%) training accuracy on MNIST, AGNews, and IMDB (resp. CUB), but generalised poorly.



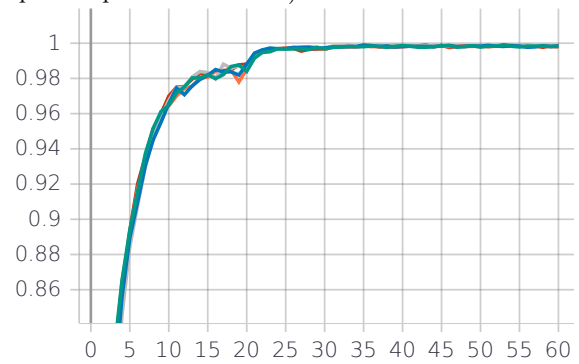
(a) Training graphs for the MNIST dataset for 5 experiments (top *train* performance 100%).



(b) Training graphs for the CUB dataset for 5 experiments (top *train* performance 94%).



(c) Training graphs for the AGNews dataset for 5 experiments (top *train* performance 100%).



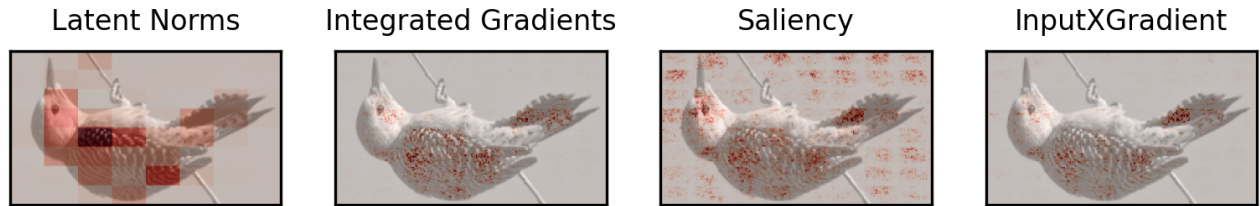
(d) Training graphs for the IMDB dataset for 5 experiments (top *train* performance 100%).

Figure 6: Training graphs for various experiments.

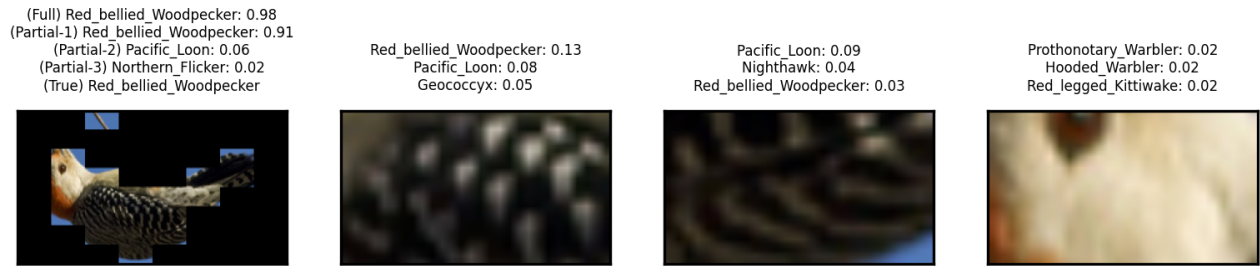
8.2 Interpretability results

8.2.1 CUB

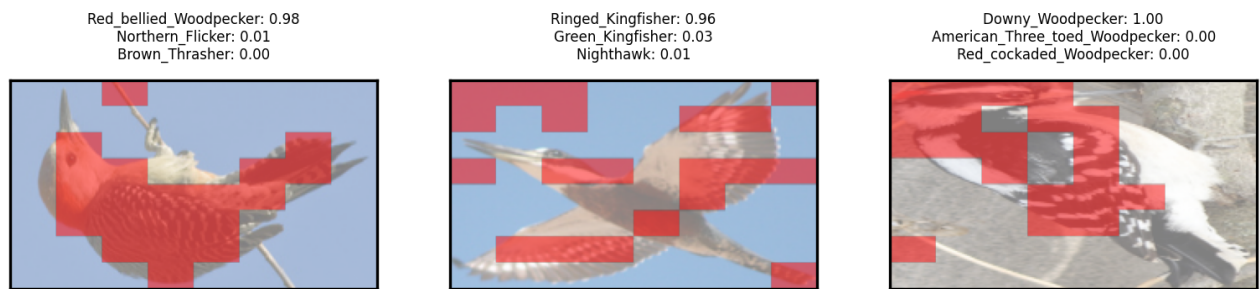
Here we show more interpretability results from the CUB dataset.



(a) Feature attribution comparisons.

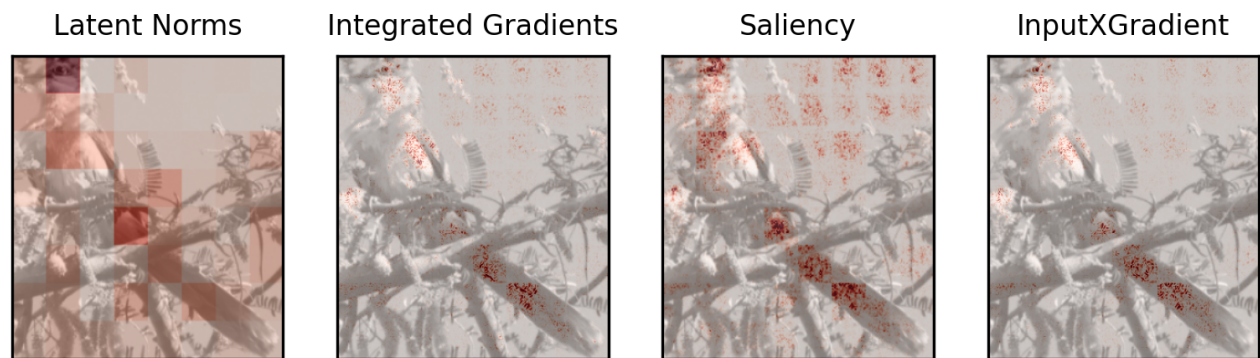


(b) Algorithmic interpretation.



(c) Example-based interpretation with correspondences.

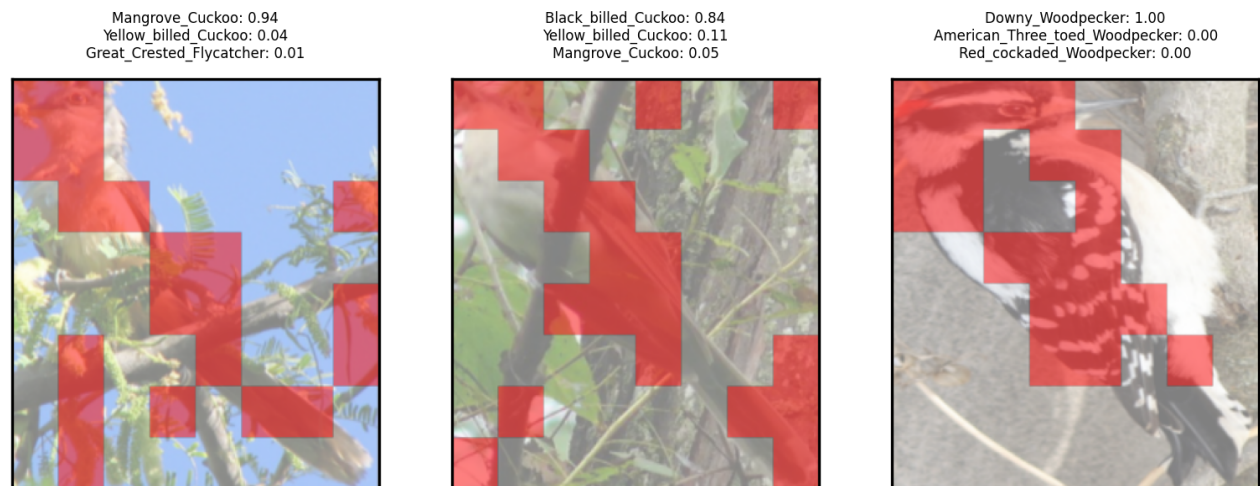
Figure 7: Additional interpretability results.



(a) Feature attribution comparisons.

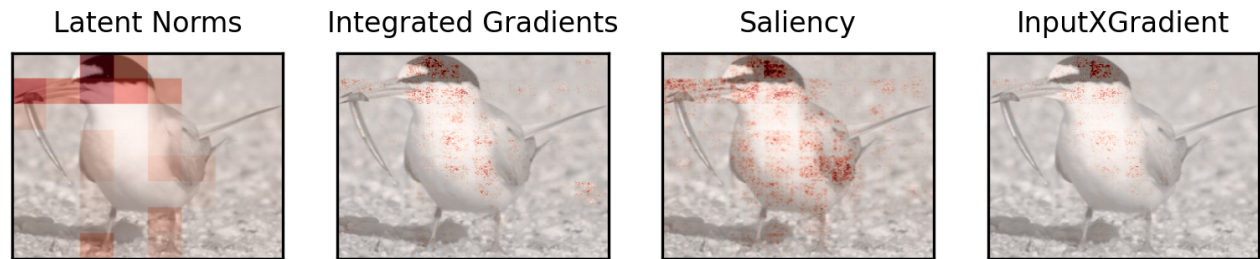


(b) Algorithmic interpretation.

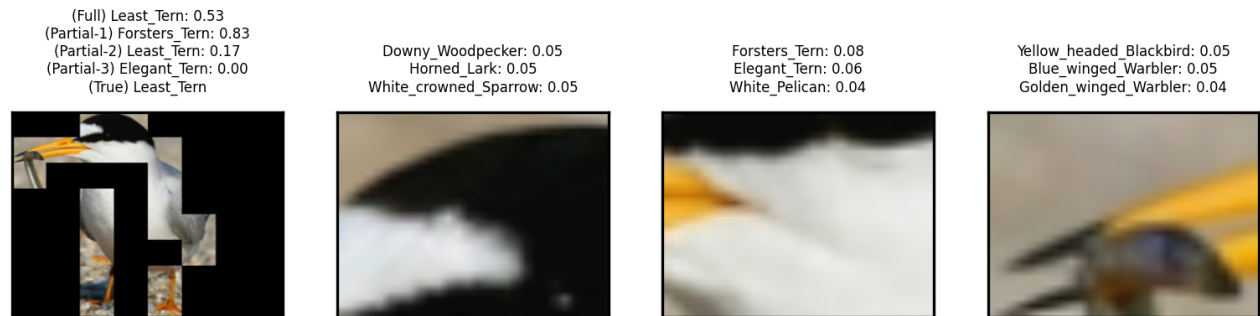


(c) Example-based interpretation with correspondences.

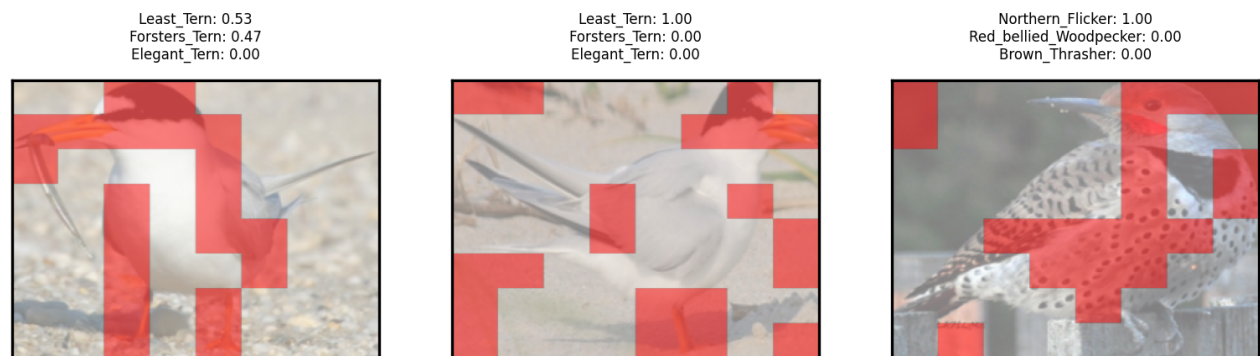
Figure 8: Additional interpretability results.



(a) Feature attribution comparisons.

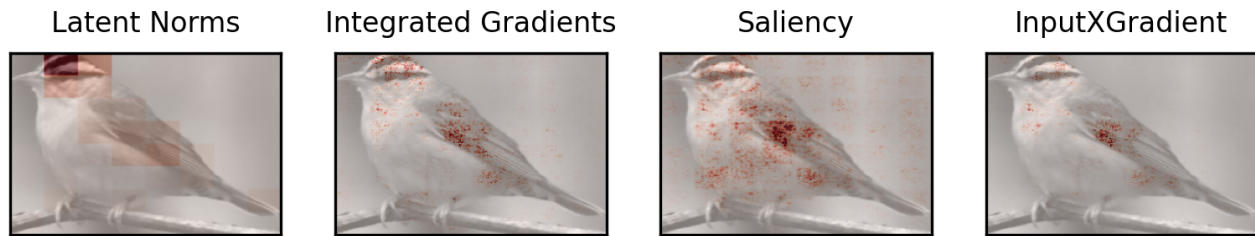


(b) Algorithmic interpretation.

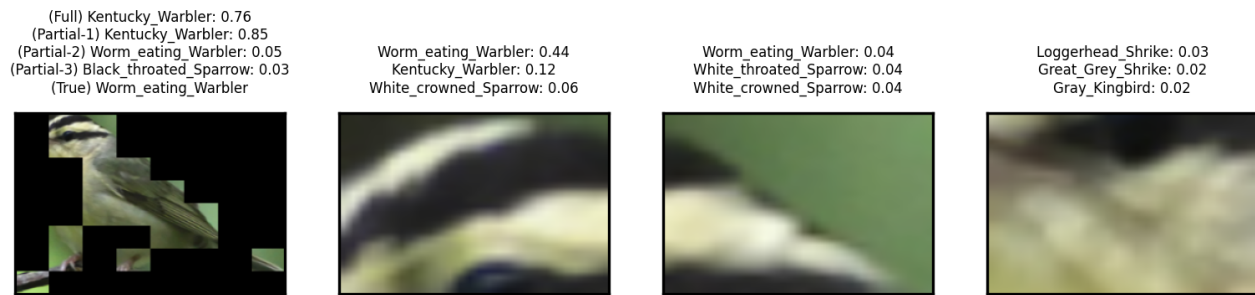


(c) Example-based interpretation with correspondences.

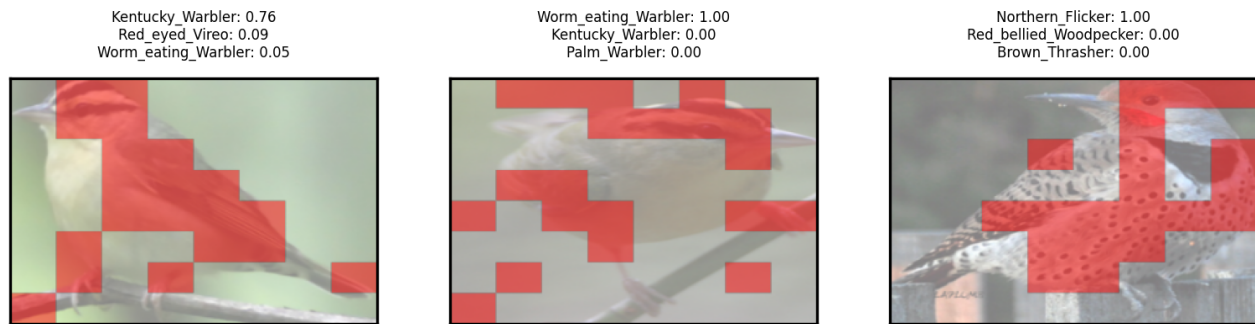
Figure 9: Additional interpretability results.



(a) Feature attribution comparisons.



(b) Algorithmic interpretation.



(c) Example-based interpretation with correspondences.

Figure 10: Additional interpretability results.

8.2.2 TCR-EPITOPE Dataset

In figure 11, we compare the interpretation of two examples by FLAN and pretrained FLAN. In FLAN the positions of the epitope sequence have considerably larger importance scores most likely due to the difference in the sequences' length, whereas pretrained FLAN manages to concentrate equally on both sequences. Furthermore, instead of considering the whole epitope sequence as important, pretrained FLAN focuses on specific positions and gives little weight to the rest.

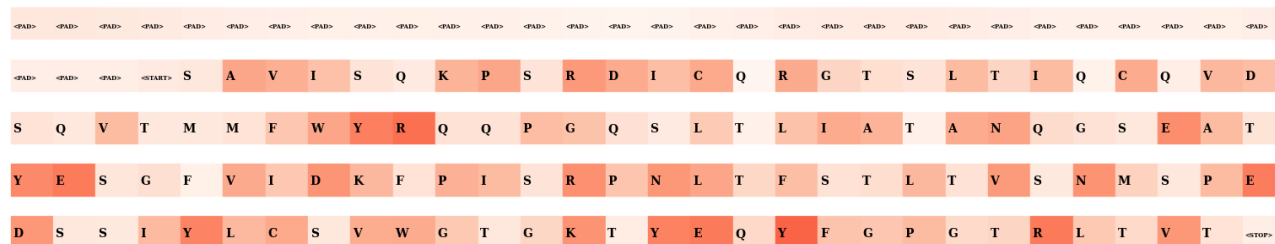
Figure 12 displays typical examples of interpreting a binding and a non-binding pair of sequences in pretrained FLAN. Both pairs have the same epitope and are classified correctly with high probability. Since the feature attributions are calculated independently for the two sequences, the epitope scores are the same in both examples. It is clear that pretrained FLAN focuses on specific positions in both sequences and in both examples. Moreover, the pretraining step suggested that certain amino acids are more important for the sequence representation, which may explain why they tend to have large scores independently of their position and the pair of sequences they belong to. For example, the "M" and "W" amino acids tend to have a very large weight in most examples and in most positions, a knowledge that is transferred to our model by the pretraining step.

Underneath each position there is its effect on the model's prediction. More specifically, let us assume we are interested in analyzing the effect of position 41 of the epitope sequence. We calculate a feature's effect by keeping all the positions of the TCR in the model and removing the remaining positions of the epitope sequence to get the binding probability predicted by the model. FLAN tends to concentrate on positions which seem irrelevant with the final prediction and also performs poorly with a linear classifier. Thus, there is evidence that the classifier is highly non-linear and the effect of each feature should not be approximated with this method.

Figure 11: Comparison between FLAN and pretrained FLAN

(a) FLAN binding pair

TCR



EPI TOPE



PREDICTION: 1 with probability: 0.844

REAL LABEL: 1

(b) FLAN non binding pair

TCR



EPI TOPE



PREDICTION: 0 with probability: 0.853

REAL LABEL: 0

TCR

<PAD>	<PAD>	<PAD>	<PAD>	<PAD>	<PAD>	<PAD>	<PAD>	<PAD>	<PAD>	<PAD>	<PAD>	<PAD>	<PAD>	<PAD>	<PAD>	<PAD>	<PAD>	<PAD>	<PAD>	<PAD>	<PAD>	<PAD>	<PAD>	<PAD>	<PAD>	<PAD>	<PAD>		
<PAD>	<PAD>	<PAD>	<START>	S	A	V	I	S	Q	K	P	S	R	D	I	C	Q	R	G	T	S	L	T	I	Q	C	Q	V	D
S	Q	V	T	M	M	F	W	Y	R	Q	Q	P	G	Q	S	L	T	L	I	A	T	A	N	Q	G	S	E	A	T
Y	E	S	G	F	V	I	D	K	F	P	I	S	R	P	N	L	T	F	S	T	L	T	V	S	N	M	S	P	E
D	S	S	I	Y	L	C	S	V	W	G	T	G	K	T	Y	E	Q	Y	F	G	P	G	T	R	L	T	V	T	<STOP>

EPITOPE

<PAD>	<PAD>	<PAD>	<PAD>	<PAD>	<PAD>	<PAD>	<PAD>	<PAD>	<PAD>	<PAD>	<PAD>	<PAD>	<PAD>	<PAD>	<PAD>	<PAD>	<PAD>	<PAD>	<PAD>	<PAD>	<PAD>	<PAD>	<PAD>	<PAD>	<PAD>	<PAD>	<PAD>	
<PAD>	<PAD>	<PAD>	<PAD>	<PAD>	<PAD>	<PAD>	<PAD>	<PAD>	<PAD>	<PAD>	<START>	L	K	E	K	G	G	L	<STOP>	<PAD>	<PAD>	<PAD>	<PAD>	<PAD>	<PAD>	<PAD>	<PAD>	<PAD>

PREDICTION: 1 with probability: 0.916
REAL LABEL: 1

(c) Pretrained FLAN binding pair

TCR

<PAD>	<PAD>	<PAD>	<PAD>	<PAD>	<PAD>	<PAD>	<PAD>	<PAD>	<PAD>	<PAD>	<PAD>	<PAD>	<PAD>	<PAD>	<PAD>	<PAD>	<PAD>	<PAD>	<PAD>	<PAD>	<PAD>	<PAD>	<PAD>	<PAD>	<PAD>	<PAD>	<PAD>	<PAD>	
<PAD>	<PAD>	<PAD>	<PAD>	<PAD>	<START>	D	A	G	V	T	Q	S	P	T	H	L	I	K	T	R	G	Q	Q	V	T	L	R	C	S
P	I	S	E	H	K	S	V	S	W	Y	Q	Q	V	L	G	Q	G	P	Q	F	I	F	Q	Y	Y	E	K	E	E
R	G	R	G	N	F	P	D	R	F	S	A	R	Q	F	P	N	Y	S	S	E	L	N	V	N	A	L	L	L	G
D	S	A	L	Y	L	C	A	S	S	L	W	G	G	N	T	E	A	F	F	G	Q	G	T	R	L	T	V	V	<STOP>

EPITOPE

<PAD>	<PAD>	<PAD>	<PAD>	<PAD>	<PAD>	<PAD>	<PAD>	<PAD>	<PAD>	<PAD>	<PAD>	<PAD>	<PAD>	<PAD>	<PAD>	<PAD>	<PAD>	<PAD>	<PAD>	<PAD>	<PAD>	<PAD>	<PAD>	<PAD>	<PAD>	<PAD>	<PAD>	<PAD>	
<PAD>	<PAD>	<PAD>	<PAD>	<PAD>	<PAD>	<PAD>	<PAD>	<PAD>	<PAD>	<PAD>	<START>	R	P	R	G	E	V	R	F	L	<STOP>	<PAD>	<PAD>	<PAD>	<PAD>	<PAD>	<PAD>	<PAD>	<PAD>

PREDICTION: 0 with probability: 0.853
REAL LABEL: 0

(d) FLAN non binding pair

8.3 Evaluation Metrics

The tables for the example-based and feature attribution metrics with the corresponding standard deviations.

Table 6: Example-Based Metrics for FLAN

	TCR-EPI TOPE		MNIST		CUB		SVHN	
	OS	LS	OS	LS	OS	LS	OS	LS
Local diversity	299.267 \pm 94.3	51.85 \pm 7.5	68.088 \pm 8.41	66.088 \pm 18.099	1507.175 \pm 270.52	1187.724 \pm 102.77	67.239 \pm 38.07	203.82 \pm 58.94
Local non-represent.	2.21 \pm 1.21	2.388 \pm 1.69	2.154 \pm 0.02	2.191 \pm 0.05	3.633 \pm 0.2	3.469 \pm 0.31	2.139 \pm 0.09	2.134 \pm 0.08
Global diversity	671.458 \pm 29.75	67.738 \pm 0.9	61.012 \pm 34.39	60.490 \pm 33.47	1376.058 \pm 3.81	1332.062 \pm 463.64	185.147 \pm 62.44	190.119 \pm 85.8
Global non-represent.	0.178 \pm 0.03	0.246 \pm 0.04	2.162 \pm 0.02	60.49 \pm 33.47	3.81 \pm 0.16	3.825 \pm 0.16	2.091 \pm 0.03	2.089 \pm 0.03

* OS: Original Space , LS: Latent Space

Table 7: Feature Metrics

(a) Monotonicity

	TCR-EPI TOPE	MNIST	CUB	SVHN
FLAN	0.173 \pm 0.14	0.1 \pm 0.08	0.024 \pm 0.03	0.043 \pm 0.03
IntegratedGradients	0.072 \pm 0.05	0.15 \pm 0.11	0.031 \pm 0.02	0.044 \pm 0.01
InputXGradient	0.071 \pm 0.05	0.16 \pm 0.1	0.044 \pm 0.03	0.026 \pm 0.02
Saliency	0.102 \pm 0.06	0.15 \pm 0.08	0.057 \pm 0.06	0.035 \pm 0.02

(b) Non Sensitivity

	TCR-EPI TOPE	MNIST	CUB	SVHN
FLAN	52.892 \pm 26.39	483 \pm 68.34	1886 \pm 2574.75	27.285 \pm 20.67
IntegratedGradients	25.191 \pm 46.12	1.83 \pm 0.98	5.4 \pm 3.13	4.571 \pm 3.95
InputXGradient	24.04 \pm 46.43	3.5 \pm 2.12	5.8 \pm 2.58	5.142 \pm 4.37
Saliency	23.502 \pm 46.93	168.85 \pm 20.32	111501.2 \pm 14985.59	1015.44 \pm 254.43

9 Supplemental files

Config files and checkpoints of trained models are available at <https://drive.google.com/file/d/1uZ33GhdCKXECH9KjfGTUpCGTAfD9yEEe/view?usp=sharing>.